# Self-Reporting Degradable Fluorescent Grafted Copolymer Micelles Derived from Biorenewable Resources

Amandine Noel,[†] Yannick P. Borguet,[†] and Karen L. Wooley*

Departments of Chemistry, Chemical Engineering, and Materials Science and Engineering, and the Laboratory for Synthetic-Biologic Interactions, Texas A&M University, College Station, Texas 77842-3012, United States

S *Supporting Information*

ABSTRACT: A series of hydrolytically degradable fluorescent poly(ferulic acid-*co*-tyrosine)-*g*-*m*PEG graft copolymers were synthesized and shown to undergo self-assembly in aqueous media to yield fluorescent micelles. The polymers and their micellar assemblies exhibited greater fluorescence emission intensity than did their small molecular building blocks, which provides a self-reporting character that has potential for monitoring the polymer integrity and also for performing in theranostics applications. The amphiphilic *graft*-copolymers were synthesized by Cu-assisted azide−alkyne "click" addition of azido-functionalized *m*PEG polymers onto fluorescent degradable hydrophobic copolymers displaying randomly distributed alkyne side-chain groups along their biorenewably derived poly(ferulic acid-*co*-tyrosine) backbones. The morphologies and photophysical properties of the supramolecular assemblies generated in aqueous solutions were evaluated by DLS, TEM, AFM, and steady-state optical spectroscopies. The 15−30 nm sized micelles behaved as broad-band emitters in the 350−600 nm range, which highlights their potential as self-reporting nanomaterials for in vitro studies.
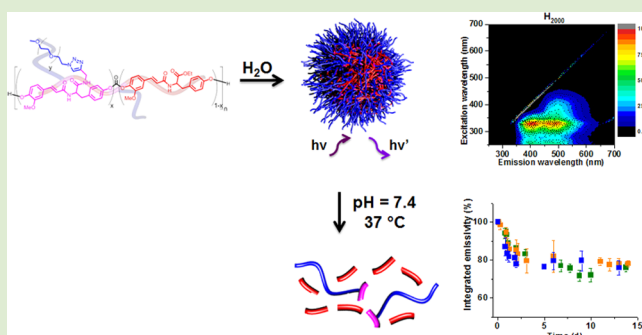

Micellar polymer nanoparticles with a core−shell structure obtained via self-assembly of amphiphilic polymers have been intensively investigated as nanomedicine devices for a wide variety of biomedical applications, such as the transport and delivery of biologically active species (drugs, nucleic acids, or proteins) to desired sites of action for the prevention, diagnosis, and treatment of diseases.[1] Polymer nanoparticles facilitate drug formulation by sequestration in their cores through hydrophobic interactions, thereby increasing the solubility of hydrophobic drugs in aqueous media and also prolonging the half-life in biological environments and enhancing binding or uptake by targeted cells. Their unique physical and chemical properties (size, shape, rigidity, and surface charge/functionality) are amenable to ample modifications and can be tuned to improve the drug carrier efficiency, according to the defined biological target.[2−5]

During the past decade, the appearance of multifunctional micellar polymer nanoparticles that are able to operate simultaneously as drug delivery vehicles and as contrast agents for imaging purposes, and coined "theranostic nanomedicines", has added a new dimension to the field of nanomedicine, as those particles enable the real-time and noninvasive evaluation of treatment response and biodistribution.[6−9] Among the different imaging modalities investigated, fluorescence-based techniques, despite their intrinsic limitations such as tissue self-fluorescence and poor tissue penetration at shorter wavelength, present a major advantage over their competitors as they do not require the use of radioactive labels (nuclear imaging), rare elements such as lanthanides (magnetic resonance imaging), or

large local concentrations of heavy elements (computed tomography). The synthesis of fluorescent polymer nanoparticles relies mostly on three distinct strategies: 1, the chemical conjugation of organic dyes[10,11] to amphiphilic polymers; 2, the encapsulation of organic dyes,[12] quantum dots (QD)[13] or fluorescent polymers[14] into the hydrophobic core of micelles; and 3, the synthesis of fluorescent amphiphilic polymers either by copolymerizing fluorescent monomers with a hydrophilic comonomer to generate brush architectures,[15−19] or through postpolymerization functionalization of a hydrophobic fluorescent polymer with a reactive hydrophilic polymer.[19,20] Each approach presents drawbacks, such as the unknown and often limited efficiency of dye conjugation reactions and tedious purification of the conjugates for the first strategy. Self-quenching of the fluorophores loaded in the core of the micelles due to concentration quenching was a major issue of the second strategy. The use of aggregation-induced emission[21] (AIE) dyes have been shown to solve this issue, however, the noncovalent nature of the labeling allows for dye leakage or surface coating detachment. The noncovalent labeling approach with QDs often present pitfalls related to toxicity.[22] Finally, the lack of degradability of the conjugated polymers that are traditionally used as building blocks in self-

Table 1. Synthetic Strategy toward Self-Fluorescent Micelles (See Also Scheme S1, SI) and Properties of *graft*-Copolymers L$_{2000}$, H$_{2000}$, L$_{5000}$, and H$_{5000}$
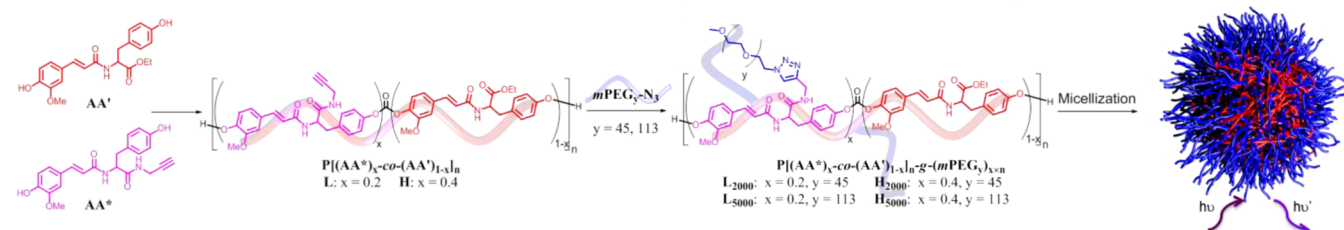
name[a]	AA′/AA*	PEG	w_{PEG}[b] (%)	T_g[c] (°C)	$D_{h(number,water)}$[d] (nm)	$D_{h(number,PBS)}$[e] (nm)	D_{TEM}[f] (nm)	λ_{ex}^{max}[g] (nm)	λ_{em}^{max}[g] (nm)
L$_{2000}$	80:20	2000	49	−5				337 (-)	420 (-)
H$_{2000}$	60:40	2000	66	−26	11 ± 3	15 ± 4	11 ± 5	341 (330)	417 (406)
L$_{5000}$	80:20	5000	71	−31	25 ± 6	25 ± 7	17 ± 6	339 (333)	417 (497)
H$_{5000}$	60:40	5000	83	−49	16 ± 4	18 ± 5	13 ± 7	346 (335)	415 (411)

[a]L and H stand for low and high grafting densities, the subscripts 2000 and 5000 correspond to the size of the *m*PEG grafts. [b]Weight fraction of *m*PEG in the copolymer, calculated as $w_{PEG} = m_{PEG}/m_{copolymer} \times 100$. [c]Determined by DSC. [d]Determined by DLS in nanopure water (5 mg·mL^{-1}). [e]Determined by DLS in PBS (1×, 5 mg·mL^{-1}). [f]Average diameter by TEM ($n = 150$). [g]Measured at a chromophore concentration of 6.59×10^{-4} M in DMF (nanopure water in parentheses).

fluorescent polymers renders those systems less attractive due to potential for biological and environmental persistence.

A major leap forward was made by Yang et al., who reported the synthesis of biodegradable photoluminescent polymers (BPLPs) with tunable emission properties from biocompatible building blocks composed of citric acid, aliphatic diols and amino acids via a polycondensation reaction.[23] More recently the same group has elaborated amphiphilic diblock copolymers via modification of the chain ends of the BPLPs and demonstrated the successful assembly of the resulting amphiphilic copolymers in aqueous solutions to generate fluorescent micelles,[24] while Gong et al. have developed a tumor-targeted fluorescent unimolecular micelle with high drug loading level and pH-controlled drug release making use of BPLPs as fluorescent building blocks.[25]

Our group has recently disclosed the synthesis of self-fluorescent and degradable poly(carbonate-amide)s obtained in only two synthetic steps from biobased L-tyrosine ethyl ester and a lignin-sourced aromatic compound: ferulic acid (FA).[26,27] We now report on our initial synthetic efforts toward the development of self-fluorescent micelles with potential for drug delivery applications.

The overall synthetic strategy toward amphiphilic graft copolymers that were capable of exhibiting self-reporting fluorescent character involved the conjugation of multiple mono chain-end-functionalized hydrophilic *m*PEGs onto the backbone of hydrophobic and fluorescent regiorandom poly-(ferulic acid-*co*-tyrosine)s. It has been demonstrated in an earlier report that regiorandom poly(ferulic acid-*co*-tyrosine)s represent an attractive platform in terms of ease of synthesis and photophysical properties, in comparison to their corresponding regioregular analogs.[27] Because of their mostly aromatic backbone, poly(ferulic acid-*co*-tyrosine)s are highly hydrophobic and can be solubilized only in a few organic solvents. To impart amphiphilic character to the poly(ferulic acid-*co*-tyrosine)s, we initially attempted to modify the phenol-functionalized chain ends to introduce reactive groups for subsequent grafting of hydrophilic polymers. This approach met with limited success due to nonquantitative functionalization of the chain ends of higher molecular weight fractions. Therefore, a *grafting-to* approach onto reactive groups along the polymer backbone was developed as an alternate strategy. A

new comonomer AA* (Scheme S2), structurally analogous to the fluorescent monomer AA′, was designed to display fluorescent properties similar to monomer AA′ and to allow further functionalization of the resulting copolymers via an efficient click-chemistry reaction between the alkyne groups from the AA* repeat unit and an azido-functionalized hydrophilic polymer. The alkyne function was introduced on the AA* monomer through a relatively stable amide linkage to prevent a fast release of the hydrophilic grafts under hydrolytic conditions. Poly(ethylene glycol) is a biocompatible and FDA approved water-soluble polymer that is known to enhance the circulation time of nanoparticles in vivo[1] and was selected to constitute the hydrophilic grafts due to its ready availability with a broad range of chain-end functionalization.

Two statistical poly(carbonate-amide)s, containing either a low (L) or a high (H) nominal fraction of alkyne groups along the polymer backbone (20 and 40%, respectively) were generated by copolycondensation of different initial feed ratios of monomers AA′ and AA* with phosgene generated in situ from diphosgene, assuming similar reactivity ratios (Table 1). The structure and purity of the copolymers were confirmed by NMR spectroscopy, size exclusion chromatography (SEC), and thermal analysis (Table 1 and SI). The relative ratio of incorporation of repeat units AA′ to AA* could not be determined directly by integration of the ^{1}H NMR spectra, due to the overlap of the characteristic resonances, however, the introduction of monomer AA* into the copolymer was confirmed unequivocally by ^{13}C NMR spectroscopy (Figure 1a, red arrows, for copolymer L, see SI for copolymer H).

Two α-azido-functionalized *m*PEG polymers of average molecular weights 2 and 5 kDa were *grafted onto* the hydrophobic polymer backbones L and H using the copper-catalyzed azide−alkyne cycloaddition reaction to afford a series of four graft copolymers with different graft lengths and densities (Table 1). The successful and quantitative PEGylation was confirmed by ^{1}H and ^{13}C NMR spectroscopies (Figures 1b and SI), as well as by SEC analysis. In particular, in the ^{13}C NMR spectra, the alkyne peaks from the AA* repeat units at 80.8 and 73.2 ppm disappeared postmodification while a strong peak centered around 71.3 ppm confirmed the presence of the *m*PEG grafts (Figure 1b). Size-exclusion chromatography analysis displayed a shift of the elution peak toward the higher
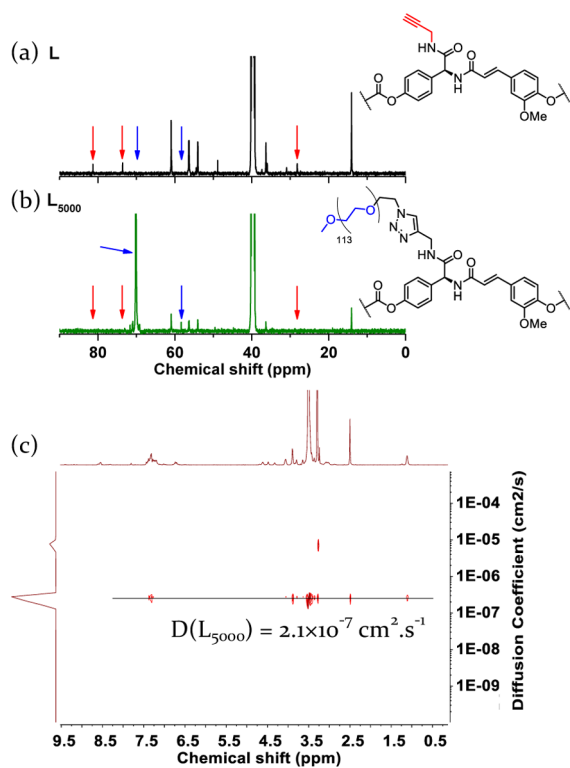
Figure 1. ^{13}C NMR spectra of **L** (a), **L$_{5000}$** (b), and DOSY spectrum of **L$_{5000}$** (c) in DMSO.

evaluated by dynamic light scattering (DLS), bright field transmission electron microscopy (TEM), and atomic force microscopy (AFM), and the surface charge densities of the nanoassemblies were measured as ζ-potential values, by electrophoretic light scattering (Table 1, Figure 2 and SI,
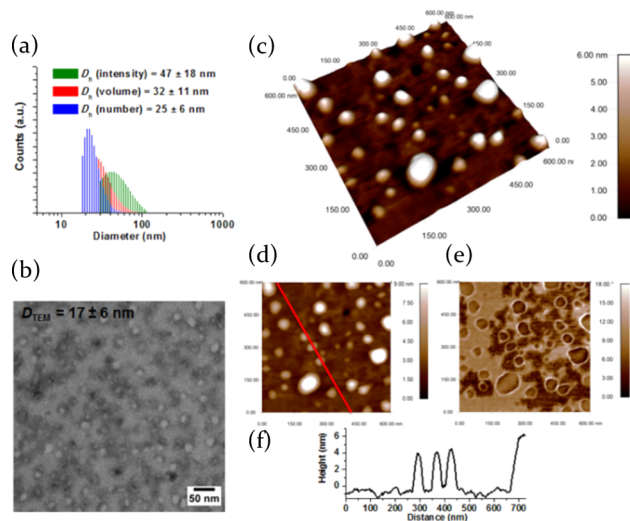

Figure 2. Characterization of the self-assemblies generated from **L$_{5000}$** in nanopure water by DLS (a); by TEM, stained with PTA (b); by AFM, three-dimensional height image (c), height image (d), phase image (e), and height profile of the cross-section in red in the height image (f).

molecular weights and the absence of residual mPEG-N$_3$ contaminant in the final products after purification (SI, Figures S1 and S2 and Table S2).[26] The successful formation of the *graft*-copolymer structures and the absence of residual mPEG-azide homopolymer in the final products were further assessed by diffusion-ordered NMR spectroscopy (DOSY)[28] (Figures 1c and SI, Table S1). The diffusion coefficients for the two mPEG-N$_3$ polymers, the starting copolymers (**L** and **H**), the resulting four *graft*-copolymers and a physical blend of the copolymers **L** and **H** with each mPEG-N$_3$ (2 and 5 kDa) are displayed in the SI and give further credit to the successful functionalization and purity of the *graft*-copolymers (Table S1). Finally, the thermal properties of the *graft*-copolymers were investigated by thermogravimetric analysis (TGA) and differential scanning calorimetry (DSC). The *graft*-copolymers displayed increased thermal stabilities over their parent copolymers, as determined by TGA (ca. 350 °C vs ca. 200 °C, respectively; SI, Figure S3 and Table S2), and that trend was linked to the weight fraction of mPEG (w_{PEG}) in the *graft*-copolymers. Similarly, the glass transition temperatures (T_g), as measured by DSC, were influenced by w_{PEG}: the higher the w_{PEG}, the lower the T_g (−5 °C for **L$_{2000}$** vs −49 °C for **H$_{5000}$**, for example).

The self-assembly behavior of the *graft*-copolymers was investigated by direct resuspension of the lyophilized samples into nanopure water or PBS (1×) at various concentrations (1, 5, and 10 mg·mL^{-1}). The hydrophilic polymer weight fraction (w_{PEG}) exerted a critical effect over the solubility of the *graft*-copolymers: **L$_{2000}$**, which possesses the lowest mPEG weight fraction, could not be resuspended directly into aqueous solutions, even at 1 mg·mL^{-1}, whereas **H$_{2000}$**, **L$_{2000}$**, and **H$_{5000}$** afforded homogeneous solutions upon sonication at room temperature. The effect of the mPEG graft densities and lengths over the morphologies of the polymer assemblies was

Figures S4−S8 and Table S3). Uniform particle suspensions were obtained for all three samples by direct resuspension in nanopure water and PBS (1×) at 5 mg·mL^{-1}, as demonstrated by the monomodal size distributions by DLS. A noticeable effect of the graft densities over the size of the assemblies, independently of the graft lengths, was observed both in solution (DLS), and in the dried state (TEM) with number-averaged hydrodynamic diameters, D_h of 32 ± 11 versus 16 ± 9 and 23 ± 13 nm, and D_{TEM} of 17 ± 6 versus 11 ± 5 and 13 ± 7 nm for polymers **L$_{5000}$** versus **H$_{2000}$** and **H$_{5000}$**, respectively. Particularly, from the TEM histogram data of Figure S7, it is apparent that high density grafting of mPEG provides for smaller assemblies than does low mPEG graft density, likely due to increased hydrophilic:hydrophobic balance, and although longer mPEG grafts would further increase the hydrophilic:hydrophobic balance, the larger volume of the longer grafts also appears to lead to a slight increase in nanoassembly dimensions. The TEM images further confirmed the uniformity of the particle sizes (Figure 2), while by AFM the particles presented a larger apparent diameter, which could be attributed to a deformation of the micelles upon deposition and drying on the glass support. This observation was confirmed by height measurements that ranged between 4 to 6 nm for all three samples. The surface charge of the assemblies was neutral with ζ-potential values between −5 and −9 mV in PBS (1×).

The critical micellar concentration (CMC) of the assemblies was evaluated through the surface tension method as determined by the pendant drop technique, due to the fluorescent properties of the *graft*-copolymers, which prohibited the use of the common pyrene assay,[29] and the inherent limitations of DOSY NMR at low concentrations.[28] The CMC values were determined from the break point of the semilogarithmic plots of surface tension vs polymer concen-

tration at room temperature. The CMC values determined by this method were similar, within experimental errors, for the three *graft*-copolymers (SI, Table S4 and Figure S9) and of about 0.2 mg·mL^{-1}, which is too high for systemic drug delivery applications, although lower CMC values could possibly be achieved in biologic media due to the salting-out effect.[30]

The photophysical properties of the *graft*-copolymers in their unimolecular (in DMF) and self-assembled states (micelles, in aqueous environment) were probed by UV–vis and fluorescence spectroscopies and compared to the properties of the parent copolymers and monomers. First, the fluorescence profiles of the different compounds were evaluated in their unimolecular states in DMF (SI, Figure S10) using multidimensional excitation/emission spectroscopy (3D fluorescence). The "fingerprints" of the electronic levels generated herein, gave similar information to the more common 2D spectra (SI, Figure S11), while facilitating the visual analysis. Monomers **AA′** (λ_{em}^{max} 392 nm, λ_{ex}^{max} 342 nm) and **AA*** (λ_{em}^{max} 392 nm, λ_{ex}^{max} 343 nm) displayed a band structure similar to FA (λ_{em}^{max} 402 nm, λ_{ex}^{max} 349 nm), but were brighter than FA (2 and 2.5×, respectively) at a chromophore concentration of 6.59×10^{-4} M (λ_{ex} 343 nm) in DMF (SI, Figure S12). Copolymers **L** and **H** were investigated under identical conditions and displayed similar fluorescence properties (emission intensities, λ_{em}^{max}, and λ_{ex}^{max}), in addition to an important red-shift of the λ_{em}^{max} (468 and 471 nm for **L** and **H**, respectively) compared to the monomers (**AA′** and **AA***, λ_{em}^{max} 392 nm; SI, Figure S13).[27] It is noteworthy that these new copolymers exhibited red-shifted fluorescence emission wavelengths to regions even more in the visible range of the spectrum (by ca. 55 nm) than the poly(ferulic acid-*co*-tyrosine) copolymers previously reported,[27] which further underlines their potential for applications as biomaterial and medical devices where unique fluorescence/contrast is necessary.[31–34] Despite the hypsochromic shift observed in both excitation and emission wavelengths upon addition of the *m*PEG grafts to the parent copolymers **L** and **H**, the emission of the *graft*-copolymers remained in the visible region of the spectrum and was not notably affected by the graft densities or lengths (Table 1). However, further analyses revealed that the relative emission intensities of the *graft*-copolymers were influenced by the *m*PEG weight fraction (Figure 3a). An increase in the graft lengths at constant grafting density (**L$_{2000}$** vs **L$_{5000}$**) or an increase of the grafting densities at constant graft length (**L$_{2000}$** vs **H$_{2000}$** or **L$_{5000}$** vs **H$_{5000}$**) led to an overall decrease of the relative emissivity of the *graft*-copolymers in DMF, at identical chromophore concentration.

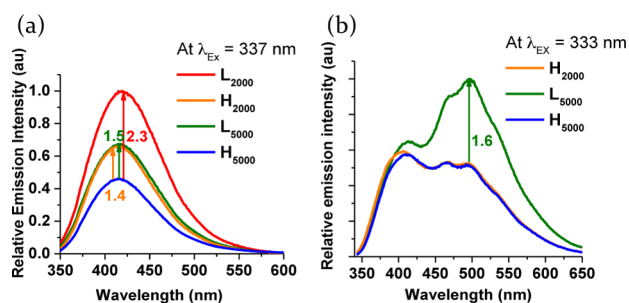**Figure 3.** Relative emission intensity spectra for the *graft*-copolymers at a chromophore concentration of 6.59×10^{-4} M in DMF (a) and nanopure water (b).

The fluorescence of the *graft*-copolymers was then investigated in aqueous solutions at a chromophore concentration of 6.59×10^{-4} M, which is well above the CMC of any of the systems. Gratifyingly, the micelles behaved as broad-band emitters in the 350−600 nm range, which makes possible their detection for imaging purposes by common optical systems that are optimized for DAPI fluorescence, an organic dye widely used as a biological stain.[35] Despite the overall similarity of the emission/excitation properties of all three *graft*-copolymers, as evidenced by 3D fluorescence, it is worth noting that **L$_{5000}$** presented an enhanced emission at 494 nm compared to **H$_{2000}$** and **H$_{5000}$** (Figure 3b and SI, Figures S14 and S15) that could potentially be attributed to a lower grafting density in **L$_{5000}$** versus **H$_{2000}$** and **H$_{5000}$**. The overlap between the emission spectra for **H$_{2000}$** and **H$_{5000}$**, which possess the same grafting density, gives further support to this hypothesis.

Interestingly, the λ_{ex}^{max} of the *graft*-copolymers in aqueous solutions displayed a concentration-dependent behavior above a given concentration, which translated into a red-shift of the maximum of excitation when increasing the polymer concentration (SI, Figure S16). This behavior is reminiscent of a CMC-like transition, whereby the physical properties of a solution are affected by the aggregation state of the solute.[30] By plotting the λ_{ex}^{max} for the successive dilutions as a function of the polymer concentration, CMC values of 0.2, 0.1, and 0.4 mg·mL^{-1} were obtained for **L$_{5000}$**, **H$_{2000}$**, and **H$_{5000}$**, respectively, which are in agreement with the CMC values determined by the surface tension method (vide supra).

The hydrolytic behaviors of the self-assembled *graft*-poly(carbonate-amide)s were evaluated in PBS buffer at 37 °C and pH = 7.4 to mimic biological environments. Fluorescence spectroscopy was used as a tool to monitor the degradation kinetics, due to the photophysical properties of the systems under investigation and the issues encountered with other techniques. To evaluate the feasibility of the study, a preliminary experiment was performed at pH = 12 on polymer **L$_{5000}$** as a model compound. The micelle solution degraded quickly under these conditions ($t_{1/2} \sim 0.5$ h, Figure 4a and SI,
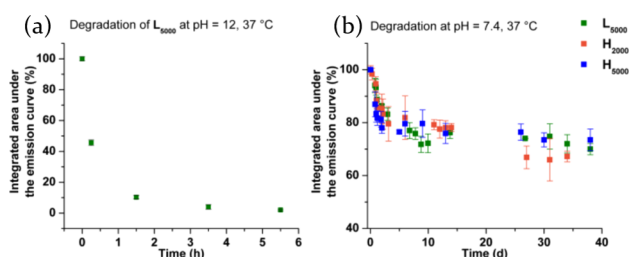

Figure 4. Evaluation of the degradation kinetics at 37 °C, pH = 12 for **L$_{5000}$** (a) and pH = 7.4 for **L$_{5000}$**, **H$_{2000}$**, and **H$_{5000}$** (b).

Figure S17 and Table S5), which contrasts starkly with the behavior of the related poly(carbonate-amide)s in the bulk that required extended incubation times (>2 weeks) at relatively elevated temperatures (70 °C) to degrade.[27] Encouraged by this result, more biologically relevant conditions were then evaluated (pH = 7.4, 37 °C). Unfortunately, one or more of the degradation products appeared to emit within the same wavelength range as the starting micelles at neutral pH, complicating the analysis of the results and leading to the presence of an offset in the degradation plots (Figure 4b). Nevertheless, a clear decrease in the emissivity of all three polymer systems was observed during the first 10 days of

incubation, after which the signal eventually plateaued. Fitting of the data was performed assuming pseudo-first-order kinetics and half-lives appeared to correlate inversely with the mPEG weight fraction (30–40 h for L_{5000} and H_{2000} vs 11 h for H_{5000}).

In conclusion, the synthesis of four degradable, self-fluorescent *graft*-copolymers derived from biorenewable resources that are capable of self-assembly behavior in aqueous solutions is described. The influence of the graft lengths and densities on the overall thermal and photophysical properties, as well as on the morphologies of the resulting self-assembled *graft*-copolymers in aqueous solutions was investigated in detail. With each nanoassembly having number-averaged hydrodynamic dimensions for the entire $D_{h(number)}$ histogram <100 nm, these materials are candidates to achieve an efficient cellular internalization (<200 nm) without being cleared too easily from the body either by filtration in the kidneys (<10 nm) or by macrophage cells of the liver and spleen (>100 nm)[36] revealing their high potential for further investigations toward drug delivery applications. Importantly, the self-fluorescent micelles displayed fluorescent emission in the visible range of the electromagnetic spectrum (350–600 nm) similar to 4′,6-diamidino-2-phenyl-indole (DAPI).[35] This work, as proof of concept for the chemistry, highlights the potential of mPEG-g-poly(ferulic acid-co-tyrosine)s as degradable self-reporting/imaging agents. The evaluation of their potential as imaging agents for in vitro applications will be reported elsewhere.

■ ASSOCIATED CONTENT

Ⓢ Supporting Information

Experimental details and complete spectroscopic, chromatographic, microscopic, and thermal analysis data for the preparation, assembly, characterization, and degradation of the monomers, polymers, and graft block copolymers. The Supporting Information is available free of charge on the ACS Publications website at DOI: 10.1021/acsmacrolett.5b00227.

■ AUTHOR INFORMATION

Corresponding Author
*E-mail: wooley@chem.tamu.edu.

Author Contributions
†A.N. and Y.P.B. contributed equally.

Notes
The authors declare no competing financial interest.

■ ACKNOWLEDGMENTS

■ REFERENCES

(1) Elsabahy, M.; Wooley, K. L. *Chem. Soc. Rev.* **2012**, *41* (7), 2545–2561.

(2) Yan, Y.; Such, G. K.; Johnston, A. P. R.; Best, J. P.; Caruso, F. *ACS Nano* **2012**, *6* (5), 3663–3669.

(3) Mout, R.; Moyano, D. F.; Rana, S.; Rotello, V. M. *Chem. Soc. Rev.* **2012**, *41* (7), 2539–2544.

(4) Chen, J.; Clay, N. E.; No-hyung, P.; Kong, H. *Chem. Eng. Sci.* **2015**, *125* (24), 20–24.

(5) Mura, S.; Nicolas, J.; Couvreur, P. *Nat. Mater.* **2013**, *12* (11), 991–1003.

(6) Lim, E.-K.; Kim, T.; Paik, S.; Haam, S.; Huh, Y.-M.; Lee, K. *Chem. Rev.* **2015**, *115* (1), 327–394.

(7) Rizzo, L. Y.; Theek, B.; Storm, G.; Kiessling, F.; Lammers, T. *Curr. Opin. Biotechnol.* **2013**, *24* (6), 1159–1166.

(8) Lammers, T.; Aime, S.; Hennink, W. E.; Storm, G.; Kiessling, F. *Acc. Chem. Res.* **2011**, *44* (10), 1029–1038.

(9) Oerlemans, C.; Bult, W.; Bos, M.; Storm, G.; Nijsen, J. F.; Hennink, W. *Pharm. Res.* **2010**, *27* (12), 2569–2589.

(10) Gonil, P.; Sajomsang, W.; Ruktanonchai, U. R.; Na Ubol, P.; Treetong, A.; Opanasopit, P.; Puttipipatkhachorn, S. *Biomacromolecules* **2014**, *15* (8), 2879–2888.

(11) Ma, X.; Wang, Y.; Zhao, T.; Li, Y.; Su, L.-C.; Wang, Z.; Huang, G.; Sumer, B. D.; Gao, J. *J. Am. Chem. Soc.* **2014**, *136* (31), 11085–11092.

(12) Yang, H.; Mao, H.; Wan, Z.; Zhu, A.; Guo, M.; Li, Y.; Li, X.; Wan, J.; Yang, X.; Shuai, X.; Chen, H. *Biomaterials* **2013**, *34* (36), 9124–9133.

(13) Lee, J.; Im, J. H.; Huh, K. M.; Lee, Y.-k.; Shin, H. *J. Nanosci. Nanotechnol.* **2010**, *10* (1), 487–496.

(14) Jung, Y.; Hickey, R. J.; Park, S.-J. *Langmuir* **2010**, *26* (10), 7540–7543.

(15) Grazon, C.; Rieger, J.; Méallet-Renault, R.; Charleux, B.; Clavier, G. *Macromolecules* **2013**, *46* (13), 5167–5176.

(16) Wu, W.-C.; Chang, H.-H. *Colloid Polym. Sci.* **2014**, 1–10.

(17) Zhang, X.; Zhang, X.; Yang, B.; Yang, Y.; Wei, Y. *Polym. Chem.* **2014**, *5* (20), 5885–5889.

(18) Shi, Y.; Cardoso, R. M.; van Nostrum, C. F.; Hennink, W. E. *Polym. Chem.* **2015**, *6*, 2048–2053.

(19) Yao, J. H.; Mya, K. Y.; Shen, L.; He, B. P.; Li, L.; Li, Z. H.; Chen, Z.-K.; Li, X.; Loh, K. P. *Macromolecules* **2008**, *41* (4), 1438–1443.

(20) Pu, K.-Y.; Liu, B. *Adv. Funct. Mater.* **2011**, *21* (18), 3408–3423.

(21) Mei, J.; Hong, Y.; Lam, J. W. Y.; Qin, A.; Tang, Y.; Tang, B. Z. *Adv. Mater.* **2014**, *26* (31), 5429–5479.

(22) Zhang, X.; Zhang, X.; Wang, S.; Liu, M.; Tao, L.; Wei, Y. *Nanoscale* **2013**, *5* (1), 147–150.

(23) Yang, J.; Zhang, Y.; Gautam, S.; Liu, L.; Dey, J.; Chen, W.; Mason, R. P.; Serrano, C. A.; Schug, K. A.; Tang, L. *Proc. Natl. Acad. Sci. U.S.A.* **2009**, *106* (25), 10086–10091.

(24) Gyawali, D.; Zhou, S.; Tran, R. T.; Zhang, Y.; Liu, C.; Bai, X.; Yang, J. *Adv. Health. Mater.* **2014**, *3* (2), 182–186.

(25) Chen, G.; Wang, L.; Cordie, T.; Vokoun, C.; Eliceiri, K. W.; Gong, S. *Biomaterials* **2015**, *47* (0), 41–50.

(26) Noel, A.; Borguet, Y. P.; Raymond, J. E.; Wooley, K. L. *Macromolecules* **2014**, *47* (9), 2974–2983.

(27) Noel, A.; Borguet, Y. P.; Raymond, J. E.; Wooley, K. L. *Macromolecules* **2014**, *47* (20), 7109–7117.

(28) Bakkour, Y.; Darcos, V.; Li, S.; Coudane, J. *Polym. Chem.* **2012**, *3* (8), 2006–2010.

(29) Silva, P. R. S.; Mauro, A. C.; Mansur, C. R. E. *J. Appl. Polym. Sci.* **2009**, *113* (1), 392–399.

(30) Patist, A.; Kanicky, J. R.; Shukla, P. K.; Shah, D. O. *J. Colloid Interface Sci.* **2002**, *245* (1), 1–15.

(31) Corr, S.; Rakovich, Y.; Gun'ko, Y. *Nanoscale Res. Lett.* **2008**, *3* (3), 87–104.

(32) Zufferey, J.; Rime, B.; Francioli, P.; Bille, J. *J. Clin. Microbiol.* **1988**, *26* (2), 175–177.

(33) Sjollema, J.; Sharma, P. K.; Dijkstra, R. J. B.; van Dam, G. M.; van der Mei, H. C.; Engelsman, A. F.; Busscher, H. J. *Biomaterials* **2010**, *31* (8), 1984–1995.

(34) Torbati, A. H.; Mather, R. T.; Reeder, J. E.; Mather, P. T. *J. Biomed. Mater. Res., Part B* **2014**, *102* (6), 1236–1243.

(35) Kapuscinski, J. *Biotechnol. Histochem.* **1995**, *70*, 220−233.
(36) Peng, H.-S.; Chiu, D. T. *Chem. Soc. Rev.* **2015**, DOI: 10.1039/c4cs00294f.